Energy Flux to a Cyclonic Eddy off Cabo Frio, Brazil

MANLIO F. MANO

Laboratory of Computing Methods in Engineering (LAMCE), Department of Civil Engineering, Alberto Luiz Coimbra Institute Graduate School and Research in Engineering (COPPE), Federal University of Rio de Janeiro (UFRJ), Rio de Janeiro, Brazil

AFONSO M. PAIVA

Department of Ocean Engineering, Alberto Luiz Coimbra Institute Graduate School and Research in Engineering (COPPE), Federal University of Rio de Janeiro (UFRJ), Rio de Janeiro, Brazil

AUDALIO R. TORRES JR.

Laboratory of Marine and Atmospheric Processes Modeling (LAMMA), Department of Meteorology, Federal University of Rio de Janeiro (UFRJ), Rio de Janeiro, Brazil

ALVARO L. G. A. COUTINHO

Center for Parallel Computing (NACAD), Department of Civil Engineering, Alberto Luiz Coimbra Institute Graduate School and Research in Engineering (COPPE), Federal University of Rio de Janeiro (UFRJ), Rio de Janeiro, Brazil

(Manuscript received 11 April 2008, in final form 26 May 2009)

ABSTRACT

To evaluate the energy flux from the mean flow of South Atlantic western boundary currents toward typical Cabo Frio eddies (at Brazilian southeast coast), the southwestern Atlantic circulation was simulated with the Princeton Ocean Model. Throughout the study period, the vertical profile of eddy available potential energy direction was monitored.

The results indicated that baroclinic instability eddies first appear in intermediate depths and then its signal propagates upward, draining energy from the Brazil Current (BC), until it reaches the surface, 30 days after its formation. The depth of eddy formation is related to the vertical profile of the mean potential vorticity cross-current gradient ($\partial\overline{q}/\partial s$). The beginning of the potential energy flux toward the perturbation and the origin of the eddy occurred at a similar depth and time.

The observed pattern suggests the following cycle: 1) a well-defined southwestward-flowing BC in the beginning of the period, with a baroclinically unstable profile of $\partial\overline{q}/\partial s$; 2) energy flux from the mean flow toward perturbation at intermediate depth; 3) current destabilization and meandering; 4) formation and growth of the cyclonic eddy; 5) potential energy flux progressively shallower; 6) propagation of the eddy signal upward; and 7) stabilization of the water column.

1. Introduction

The upper-ocean circulation in the western South Atlantic, off the Brazilian coast, is characterized by the flow of two opposing and relatively intense boundary currents along the slope region. The Brazil Current (BC) flows in the south-southwest direction, from the surface until depths of approximately 450–750 m (Campos et al. 1995; da Silveira et al. 2004), closing the subtropical gyre. Below this level, down to about 1500–1800 m, the intermediate western boundary current (IWBC) flows to the north, carrying primarily low-salinity Antartic Intermediate Water. The circulation associated with these two currents has been referred to as the BC–IWBC system (da Silveira et al. 2004).

Near Cabo Frio (CF) at 23°S, the Brazilian coast changes direction abruptly (Fig. 1) in a region of relatively

Corresponding author address: Dr. Manlio F. Mano, LAMCE/COPPE/UFRJ, Av. Athos da Silveira Ramos, 149, Centro de Tecnologia – Bloco I – sala 214, Cidade Universitária, Rio de Janeiro, Brazil, CEP 21941-909.
E-mail: manlio@lamce.coppe.ufrj.br

DOI: 10.1175/2009JPO4026.1

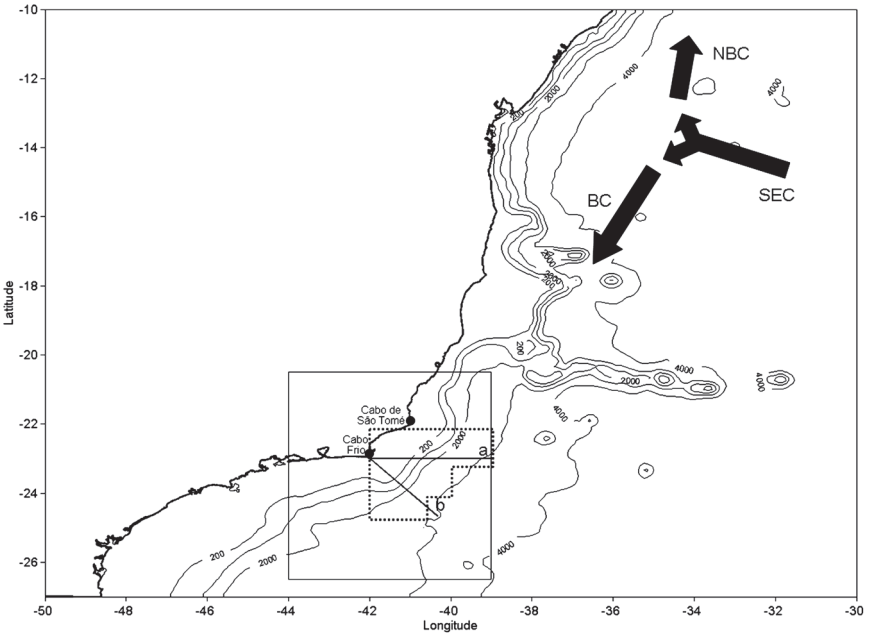

FIG. 1. Area modeled by the POM with the respective bathymetry; the rectangle highlights the area of interest of this work where the direction of the coastline changes from NE–SW to E–W, off Cabo Frio. The bifurcation of the South Equatorial Current (SEC), originating the Brazil Current (BC) and the North Brazil Current (NBC), is represented schematically.

intense mesoscale activity. A first description of the BC meandering and the formation of cyclonic and anticyclonic eddy structures off CF has been presented by Mascarenhas et al. (1971). Since then, several instances of BC eddies, meanders, and recirculation cells have been reported in this region in the scientific literature (Signorini 1978; Reid 1989; Peterson and Stramma 1991; Lorenzzetti et al. 1994; Campos et al. 1995; Stevenson 1996). The most preeminent feature, which is quite often observed in satellite images (e.g., Garfield 1990), is the meandering of the BC to the southeast of CF and the subsequent formation of a cyclonic eddy (Fig. 2) that propagates southwestward and is, at times, eventually shed from the BC axis.

Campos et al. (1995, 1996) suggested that the BC meandering is due to variations in the depth of the water column. According to the authors, the sudden change in coastline orientation at CF, associated with the potential vorticity conservation along the slope region, generates a topographic Rossby wave that propagates in the southwestern direction. Based on SST satellite images in which cyclonic and anticyclonic meanders were observed, da Silveira et al. (2000) claim that the beginning of the eddy activity actually occurs north of CF at 22°S, off Cabo de São Tomé. The meander growth and the eddy formation would arise from a baroclinic instability process within the BC–IWBC system (da Silveira et al. 2008). Following these results, the origin of the meanders would be associated with the influence of coastline orientation and bathymetry, but the eddy formation and growth would depend on a baroclinic instability process, capable of transferring available potential energy (APE) from the mean flow to the eddy field.

To the best of our knowledge, however, no studies exist, so far, characterizing the energy flux associated with the baroclinic instability for this region. The objective of the present study is, therefore, to evaluate the APE flux between the mean and the eddy flows, characteristic of baroclinic instability, and to evaluate its relation with the origin and growth of the cyclonic eddy that is formed at CF. Since direct measurements in this region are few, the problem is approached by means of high-resolution regional numerical modeling, using the Princeton Ocean Model (POM) (Blumberg and Mellor 1987).

The article is organized as follows. In section 2, the model configuration is presented, and its capacity to reproduce the main oceanographic features in the region is assessed. In section 3, the conditions for instability and the mathematical formulation considered in order to evaluate the APE fluxes are described. The APE fluxes are diagnosed during an eddy formation event, and shown in section 4. The results are then discussed and the main conclusions presented in section 5.

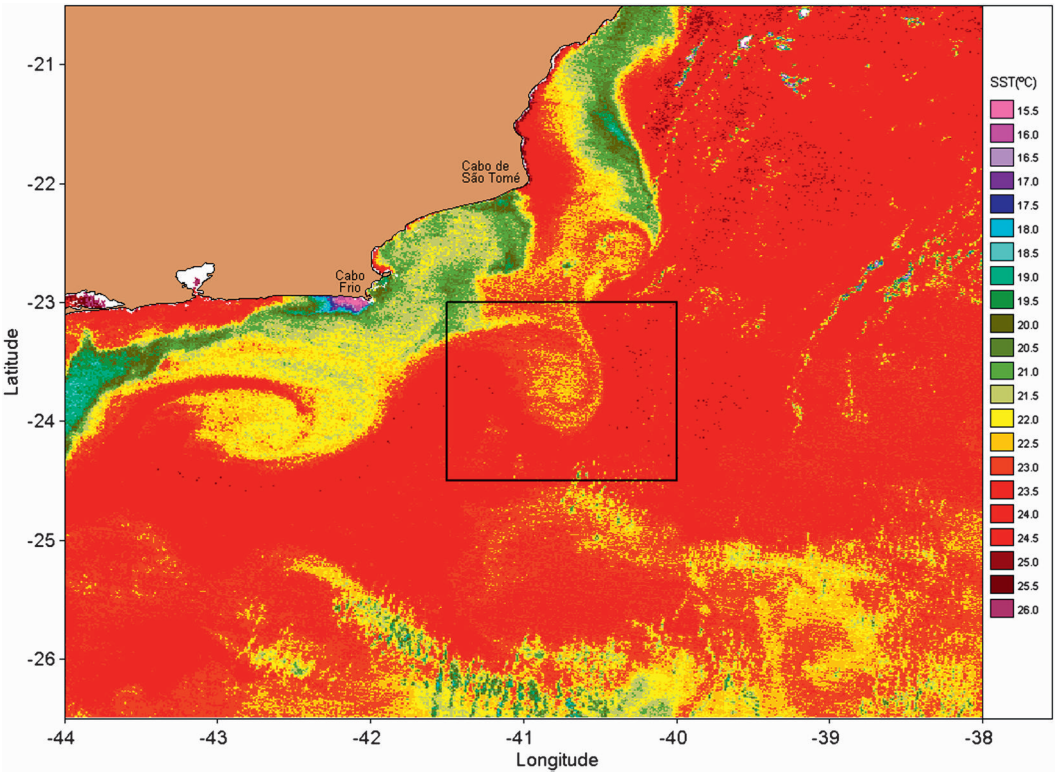

FIG. 2. SST image of the area of interest. Red tones represent the BC, which flows in the NE–SW direction, with some eddy activity. It is possible to observe three eddy formations at the western boundary of the BC. The rectangle highlights the CF eddy. Source: NOAA (http://www.nsof.class.noaa.gov).

2. Hydrodynamic modeling

a. Model configuration

To reproduce the local circulation, a 3-yr simulation was performed with POM (stabilization of kinetic energy occurs in less than 30 days). A 45-day period, in which the formation of a cyclonic eddy to the southeast of CF is well simulated, was chosen for analysis. Lateral boundary conditions were kept constant throughout the entire simulation and momentum, heat, and mass fluxes were neglected at the surface so as to guaranty that all variations in potential and kinetic energy occur essentially by internal instability processes.

The modeled domain is bounded by 10° and 27°S, 30° and 50°W (Fig. 1). The area considered is much larger than the area of interest, in order to simulate the BC from its origin and to isolate the CF region from boundary effects. The horizontal grid is regular, with 5′ resolution in latitude and longitude and a total of 241 by 205 points. This resolution is at least three times smaller than the region's internal Rossby radius of deformation. Considering the CF cyclonic eddy presented in Fig. 2, this resolution is at least eight times smaller than the eddy diameter and suffices to resolve the mesoscale at this region. Fifteen sigma levels were used in the vertical so as to resolve the vertical shear between BC and IWBC, which is an essential condition to study the baroclinic instability.

Bathymetry was based on the 5′ gridded elevations/bathymetry for the world (ETOPO5) international database (NOAA 1988). Initial conditions were derived from the Ocean Circulation and Climate Advanced Modeling (OCCAM) global model simulation (Gwilliam 1995), corresponding to the April 1996 monthly temperature and salinity means. Barotropic velocity boundary conditions were based on Flather (1976), while for the baroclinic velocity the Sommerfeld (1949) radiation conditions were used. The temperature and salinity boundary conditions followed the scheme used by Zavatarelli and Mellor (1995). The same boundary condition schemes were applied at the north, south, and east boundaries.

POM is a three-dimensional nonlinear model that integrates the primitive equations by the finite difference method using sigma coordinates in the vertical. It was designed to simulate ocean and coastal currents, being capable of appropriately resolving the nonlinear processes of the eddy dynamics. The greatest benefit of the sigma-coordinate models is related to the smooth

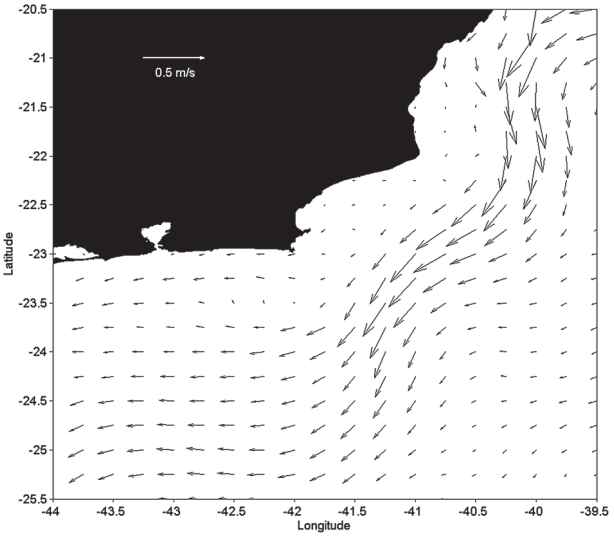

FIG. 3. Surface time-averaged velocity field (m s^{-1}), considering two years of POM simulation.

representation of topography and the ability to simulate the interaction between flow and bathymetry (Ezer et al. 2002). The disadvantage is the generation of spurious pressure gradient velocities. Tests were performed to evaluate this error in our configuration, according to Barnier et al. (1998). The magnitude of the spurious currents was found to be always lower than 10% of the total current.

b. Model evaluation

The mean surface velocity field of the last two years of simulation is presented in Fig. 3. The BC is seen with a mean axis in the northeast–southwest direction until approximately 24°S, turning westward after passing CF, and velocities around 0.35 m s^{-1}. Observations offshore from CF (da Silveira et al. 2008) show a southwestward BC at 22.7°S, 40.2°W with a mean velocity in its core of 0.41 m s^{-1}.

A zonal section at CF (section a in Fig. 1) of model mean temperature and salinity (Fig. 4) shows a vertical water mass distribution that is in agreement with the literature (Campos et al. 1995; Signorini 1978). Warm tropical water (TW) can be observed to approximately 200 m deep, followed by a sharp thermocline with temperatures decreasing from about 18° to 6°C down to ~800 m, composed of South Atlantic Central Water (SACW) and Antarctic Intermediate Water (AAIW), identified by the characteristic salinity minimum around 1000 m deep.

The simulated time-averaged flow of the BC–IWBC system is presented in Fig. 5 for a northwest–southeast oriented section beginning at CF (section b in Fig. 1).

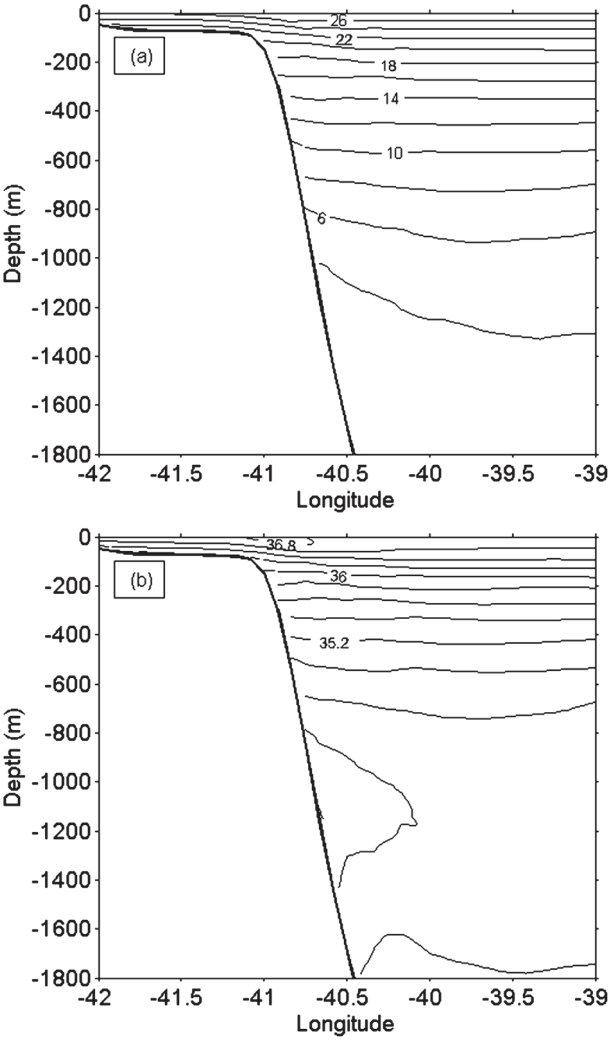

FIG. 4. Vertical sections at 23°S (section a in Fig. 1) of time-averaged (a) temperature (°C) and (b) salinity (psu), considering 2 years of POM simulation.

The inversion in the flow direction occurs, on average, around 700 m deep, varying throughout the simulation between 180 and 1000 m. Da Silveira et al. (2004), based on current (18–19 April 1983) and CTD (July 2001) data, describe the BC–IWBC as presenting a flow inversion around 450 m deep. The simulated IWBC core oscillated between 600 and 1600 m deep, with an average thickness of 1500 m and maximum averaged velocities of ~0.20 m s^{-1}. These results are also in agreement with observations made by da Silveira et al. (2004), which show the IWBC with a thickness of about 1200 m and maximum velocities of 0.30 m s^{-1} at its core, located at ~800 m deep.

In an extensive literature review, da Silveira et al. (2000) describe a BC at CF with intensive meandering activity, maximum surface velocities ranging from 0.19

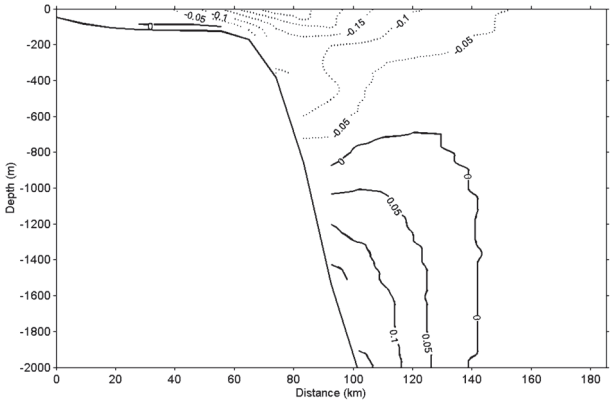

FIG. 5. Vertical section of the current (m s^{-1}) between CF and 24.67°S, 40.33°W (section b in Fig. 1). This section is NW–SE oriented, owing to the BC mean pattern in the NE–SW direction. The BC–IWBC system is presented: BC in the surface layer with negative velocities (southwestward); IWBC in the intermediate layer with positive velocities (northeastward).

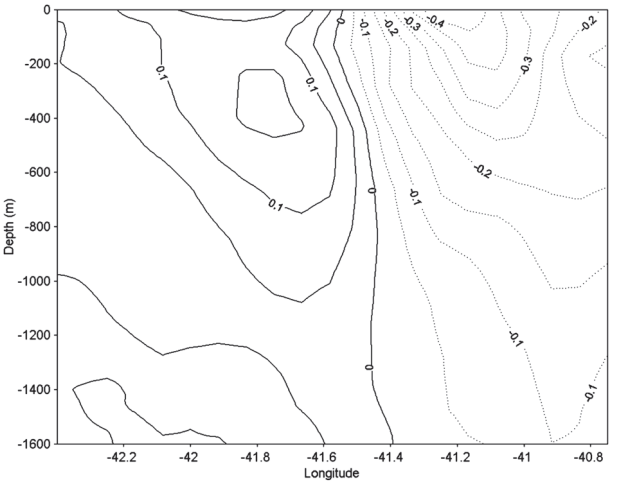

FIG. 6. Vertical section of the component v of the velocity (m s^{-1}) in the eddy region, referring to the latitude of its nucleus on the surface.

to 0.75 m s^{-1}, and transport varying from 2.2 to 11 Sv (Sv $\equiv 10^6$ m^3 s^{-1}). During the 45-day period used for the flux analysis, the simulated BC presented maximum surface velocities of 0.50 m s^{-1}, with volume transport at latitude 23°S remaining between 3.8 and 7.4 Sv.

The diameter and depth of the simulated eddy for the CF region were approximately 68 km and 800 m (Fig. 6), which agrees well with the literature (Signorini 1978; Lorenzzetti et al. 1994; Schmid et al. 1995) and SST images of this region (Fig. 2).

3. Baroclinic instability and energy fluxes

The model results were analyzed within the framework of linear theory for baroclinic instability. The vertical structure of the mean flow of the BC–IWBC system was investigated to verify the existence of necessary conditions for instability. The theory of evaluation of the instability conditions can be obtained in Johns (1988) and da Silveira et al. (2008). In summary, if the vertical profile of cross-current gradient of mean potential vorticity ($\partial\overline{q}/\partial s$) changes sign along depth, all necessary conditions are satisfied.

Despite that mean potential vorticity includes a term related to horizontal shear [see Eq. (1)], the focus here is on the vertical shear, as the objective is to investigate the development of the baroclinic instability. This specific interest in vertical shear is due to the fact that the importance of baroclinic instability to the growth of perturbations in this region was recently assessed by da Silveira et al. (2008), who concluded that the Brazil Current system is likely baroclinically unstable. Da Silveira et al. (2004) have also shown that the BC system is 75%–80% baroclinic. Thus, in Eq. (2), a baroclinic $\partial\overline{q}/\partial s$, proportional to the vertical gradient of along-current velocity, is determined from

$$\overline{q} = \nabla^2\overline{\psi} + \frac{\partial}{\partial z}\left(\frac{f^2}{N^2}\frac{\partial\overline{\psi}}{\partial z}\right) + \beta_0 y \qquad (1)$$

as

$$\left.\frac{\partial\overline{q}}{\partial s}\right|_{\mathrm{BCL}} = \frac{\partial}{\partial z}\left(\frac{f^2}{N^2}\frac{\partial\overline{v}_L}{\partial z}\right), \qquad (2)$$

where q is potential vorticity, ψ the streamfunction, f the Coriolis parameter, β the meridional gradient of f, N^2 the square of the Brunt–Väisälä frequency, and v_L is the longitudinal current (i.e., the along-current axis velocity); the overbar indicates time averaging.

Therefore, an evaluation of the vertical profile of $\partial\overline{q}/\partial s$ was made. Figure 7 shows the result for the point 24°S, 41°W considering the current axis in the southwest direction. The values of current, temperature, and salinity used to calculate N^2 and v_L are time averaged during two years of POM simulation in Fig. 7a. It should be noted that the $\partial\overline{q}/\partial s$ profile changes sign, presenting a positive peak in the upper layer (400 m) and a negative peak in the intermediate layer, around 600–700 m, confirming that the system is potentially baroclinically unstable. These depths were chosen to plot the results (Figs. 9–13). A shorter time average, from day 10 to day 30 of the study period, of current, temperature, and salinity was used in Fig. 7b so as to associate $\partial\overline{q}/\partial s$ with the energy flux.

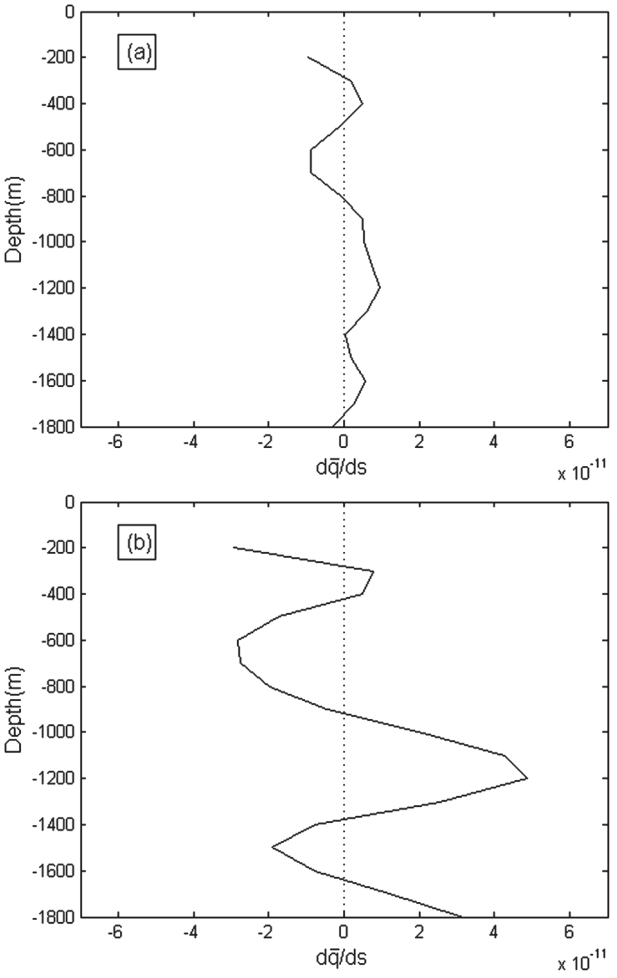

FIG. 7. Vertical profile of the cross-current gradient of the mean potential vorticity, $\partial\overline{q}/\partial s$ [(m s)$^{-1}$ × 10^{-11}], at 24°S, 41°W considering a (a) 2-yr time average and (b) a shorter time average including day 10 to day 30 of the study period. The objective is to confirm the existence of sign changes along depth. The depth layer of negative peak is related to the APE flux peak to the eddy.

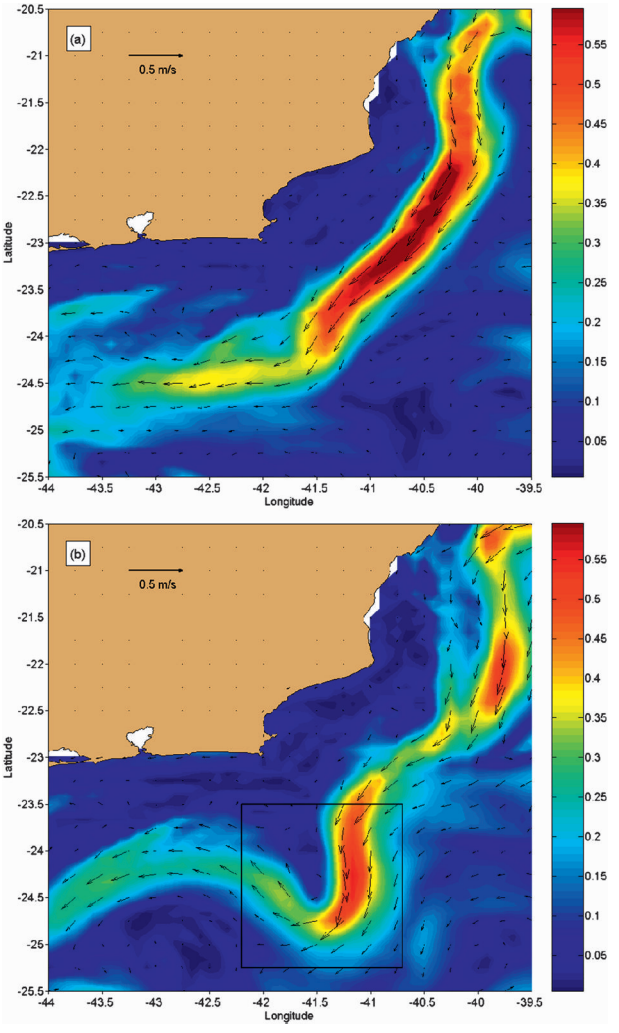

FIG. 8. Surface total velocity fields on days (a) 1 and (b) 45 of the study period simulation. The colors indicate magnitude (m s^{-1}) and vectors indicate direction. The higher magnitudes are from BC. The rectangle highlights the CF eddy signal at sea surface simulated by the POM.

Physically, the variations in vertical stretching and squeezing of fluid, imposed by the perturbation, generate new relative vorticity. However, the perturbation growth and the formation of eddies depend on the potential energy flux coming from the mean flow. Thus, in addition to the favorable conditions for instability development, an APE flux, from the current to the perturbation, is necessary. Obviously, the perturbation will not increase indefinitely because, after a certain point, nonlinear processes gain importance (dissipating this energy) and the theory used so far does not apply. When the APE flux reverses, from the perturbation to the mean flow (from eddy to the BC), weakening of the eddy and the reintensification of the current are expected.

As the increase in the perturbation field occurs to the south of CF, where the BC flows in a northeast–southwest orientation, it is important to consider the energy transfer related to the zonal and meridional velocity components. By adapting Pedlosky's (1979) derivation from one to two components of the flow and simplifying the resulting equation, looking for APE flux sign estimate, one obtains

$$\frac{\partial E}{\partial t} \sim \left[-u'T' \frac{\partial \overline{T}_y}{\partial x} - v'T' \frac{\partial \overline{T}_x}{\partial y} \right] = E_{\text{var}}, \qquad (3)$$

where E is the APE of the perturbation and T is potential temperature. The expression between brackets will be denoted by E_{var}, which gives an indication of the APE flux direction. The overbar indicates axis averaged (x or y).

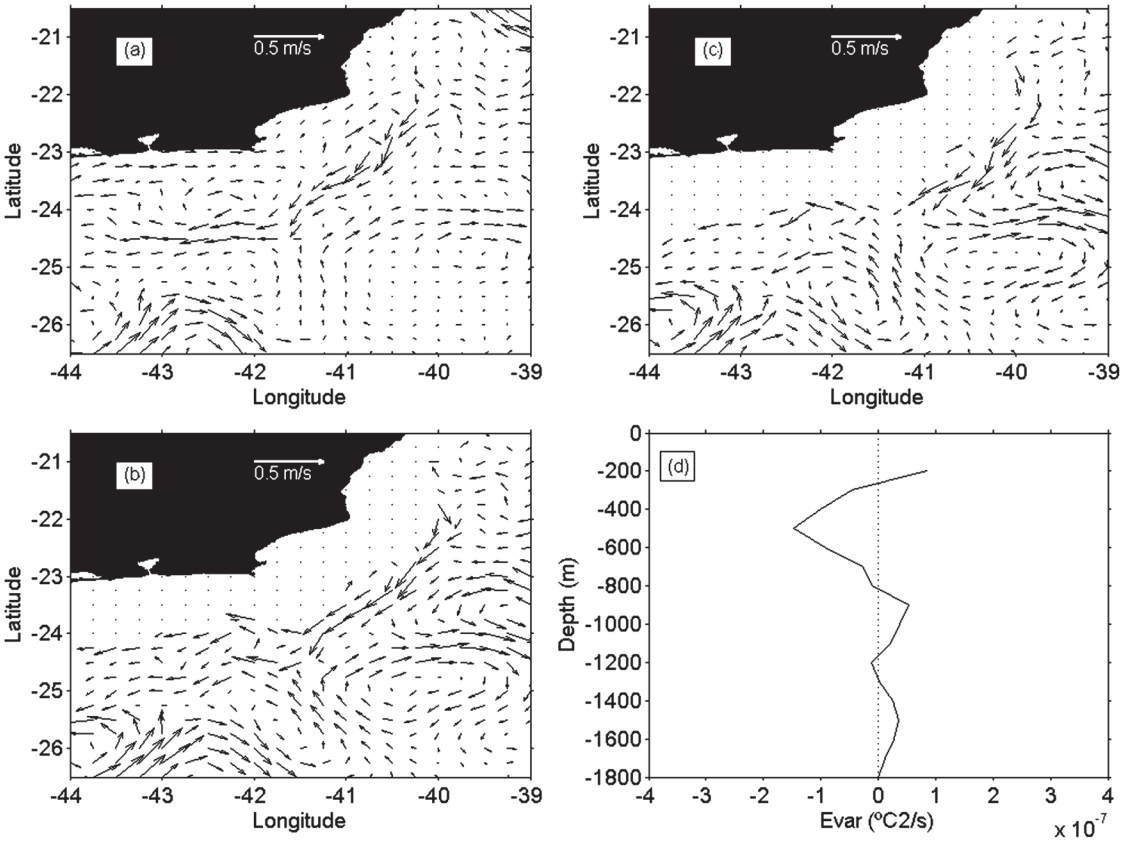

FIG. 9. Physical diagnostic for day 1 of the simulation: map of (a) the surface eddy field, (b) the eddy field at 400 m, and (c) the eddy field at 700 m; (d) vertical profile of E_{var} (normalized for the dotted polygon area in Fig. 1), in $^{\circ}\text{C}^2\ \text{s}^{-1} \times 10^{-7}$.

Monitoring of the vertical profile of E_{var} becomes, therefore, very useful. In the regions in which its sign is positive, the APE increases, meaning APE flux from the mean flow to the eddy field. When the sign of E_{var} is negative, the energy flux is reversed, from the eddy to the BC.

4. APE fluxes

In the presentation that follows regarding the APE fluxes, model days will be referenced to the beginning (day 1) of the 45-day period considered for the analysis, which covers the entire process of eddy formation at CF. At day 1 (Fig. 8a), the BC instantaneous flow, although more intense and narrow, resembles the mean flow in terms of horizontal structure and flow direction. No meander or eddy is presented at CF, where the flow follows a well-defined southwestward path. But, at day 45 (Fig. 8b), the cyclonic eddy signal can be seen at the surface, as discussed latter. What happened during these 45 days that makes BC basic flow evolve to a cyclonic eddy?

To answer this question, the following parameters were monitored and are presented for days 1, 10, 20, 30, and 40: vertical profiles of E_{var} (normalized by the number of points in each depth) in the area within the dotted polygon in Fig. 1 and eddy velocities at depths 0, 400, and 700 m. The northern limit is located at the beginning of the eddy activity in the region offshore from Cabo de São Tomé (following da Silveira et al. 2000) and the area extends to the southern limit of the simulated eddy. The meridional extension is longer than the wavelength of the most unstable waves in the region [~250 km, according to da Silveira et al. (2008)]. The variation of the eastern limit was intended to avoid the influence of other eddies that grow throughout the study period. The depths were chosen based on the vertical profile of $\partial\overline{q}/\partial s$ (Fig. 7a). Eddy velocities correspond to the instantaneous velocity minus the time-averaged velocity field computed from the last two years of simulation. Results are shown in Figs. 9–13 and are discussed below.

At day 1 (Fig. 9), the BC is very intense and the energy flux vertical profile predominantly negative above 900 m, indicating energy flux toward the mean flow. At day 10 (Fig. 10), there is a small positive peak of E_{var} at 700 m, indicating some eddy activity. This is confirmed by the

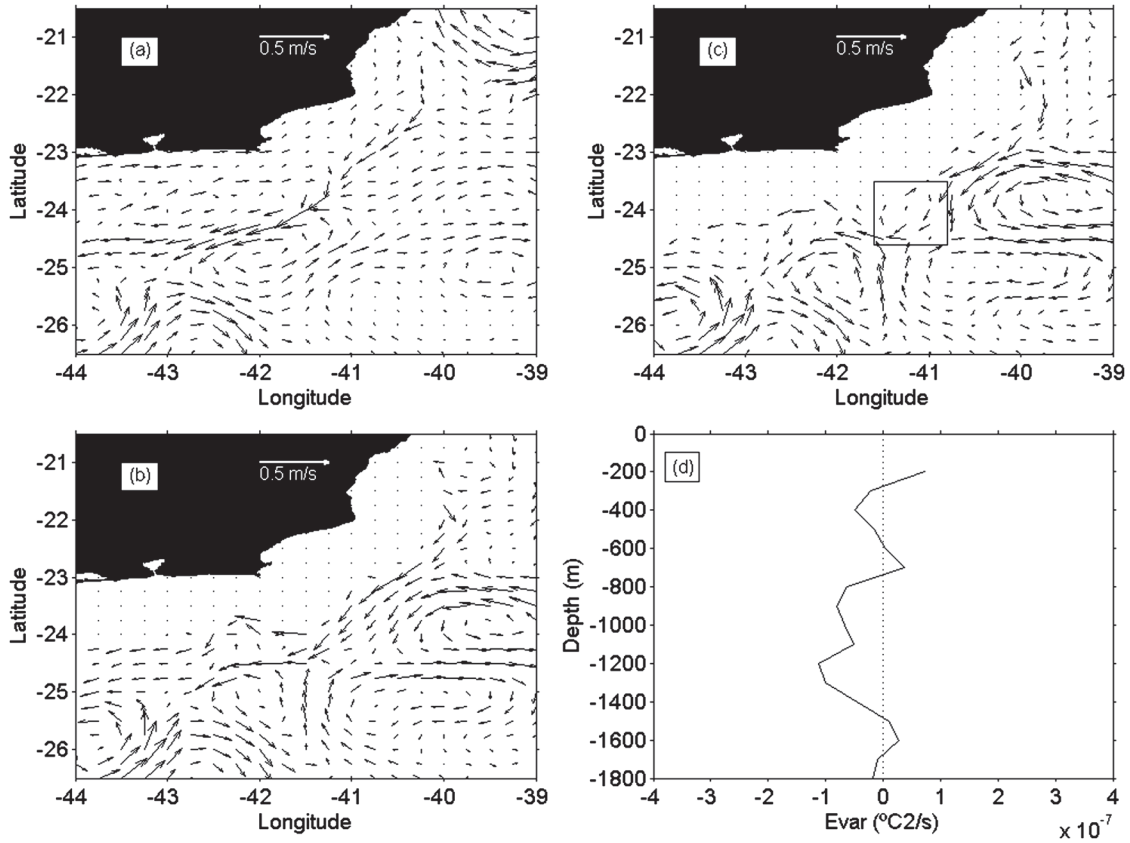

FIG. 10. As in Fig. 9, but for day 10 and in $°C^2\ s^{-1} \times 10^{-5}$. The rectangle highlights the eddy at 700 m.

eddy velocity field, in which it is possible to observe a cyclonic circulation at 700 m (Fig. 10c), southeastward of CF, indicating the formation of the eddy. It is interesting to note that no clear signal of this eddy can be seen at upper levels (Figs. 10a,b).

The maximum energy flux from the mean flow to the perturbation can be seen in day 20 (Fig. 11). Positive E_{var} values are observed between 300 and 1000 m, with a strong peak at 600 m. This depth corresponds to the layer of negative $\partial\overline{q}/\partial s$ in the water column (Fig. 7b). The cyclonic eddy is now clearly observed at 700 m. A weak signal of the cyclonic circulation can also be observed at 400 m, but is absent in the surface field.

The energy flux to the perturbation occurs in the first 800 m of the water column at day 30 (Fig. 12), and its vertical profile is more spread over lower depths. The eddy, still a dominant feature at 700 m (Fig. 12c), is now also evident at 400 m (Fig. 12b), but still cannot be discerned in the surface velocity field.

At day 40 (Fig. 13), stabilization of the intermediate layers is already observed to occur with energy fluxes toward the mean flow at lower levels. At the surface layer, however, the energy flows from the mean to the perturbation, and the cyclonic eddy is finally observed in the surface velocity field. Day 40 marks the arrival of the eddy signal at the surface, 30 days after it was first observed at 700 m.

It can be seen in Figs. 13a–c that the center of the eddy is dislocated to the southwest as we go deeper in the water column. Another interesting observation is that, despite the eddy core not being at the same location at the three depths on this particular day, one can observe in Figs. 10c, 12b, and 13a that the eddy was formed in the same location (24°–24.5°S, 41°–41.5°W) at all depths. After being formed at intermediate depth the eddy is advected southwestward, with its vertical axis tilting in the opposite direction and against the mean shear as it progressively reaches shallower depths. This tilt is required to drain energy from the mean flow (Pedlosky 1979).

This pattern is clearer in Fig. 14, which shows the time evolution of area-averaged (between 24° and 24.5°S, 41° and 41.5°W where the eddy is observed to arise at the three levels) relative vorticity profiles. The origin of the eddy at intermediate depth is evident. It is possible to notice that the negative relative vorticity (cyclonic) signal increases initially at 750 m, presenting maximum values between days 20 and 30 at depths 600 and 700 m, and progressively propagates upward.

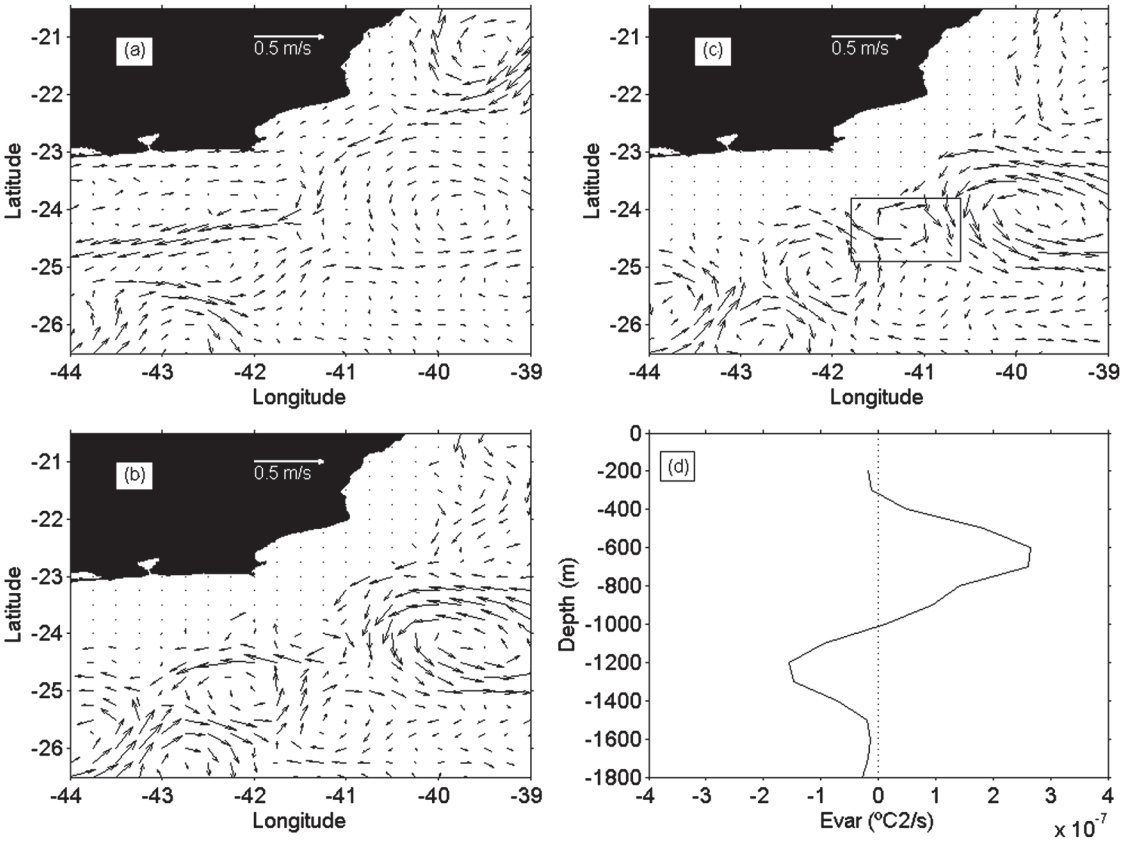

FIG. 11. As in Fig. 9, but for day 20. The rectangle highlights the eddy at 700 m. It is possible to see the perturbation growth (as a meander) at 400 m, but not as an eddy yet.

To provide a better characterization of the energy flux from the mean flow to the perturbation, the time evolution of the area-averaged E_{var} vertical profiles is shown in Fig. 15. It is possible to observe positive values of E_{var} (flux to the perturbation) before day 10, around 700 m (allowing the eddy visualization in Fig. 10c), but its positive peak occurred on day 18 at 600 m. From day 25 on, the APE flux to the perturbation was progressively shallower, reaching the surface around day 40. High values of E_{var} were observed also at the surface layer (not shown), possibly related to surface boundary instability. However, as the origin of the eddy was clearly at intermediate depth (based on Figs. 9–14, no eddy structure could be identified before day 30 at the surface layer), we focused the analysis on the internal baroclinic instability for depths below 150 m.

Comparing Figs. 14 and 15, one concludes that the energy flux to the perturbation and the eddy formation depth are within the layer of negative $\partial\overline{q}/\partial s$ (Fig. 7). The E_{var} positive peak and the relative vorticity negative peak are at a similar depth (600–700 m), but the former occurs a few days earlier. This depth is the same as the $\partial\overline{q}/\partial s$ negative peak for the period of maximum energy flux (Fig. 7b).

5. Discussion

The objective of this study was to evaluate the potential energy fluxes between the mean flow and the perturbation associated with the formation of a cyclonic eddy at CF to investigate the process of the eddy growth and its relationship to baroclinic instability. Results from a high-resolution numerical simulation made with the Princeton Ocean Model (POM), configured for the study area, were used in the analysis.

The cyclonic eddy first appears around 650 m. This depth is within the layer of negative mean potential vorticity cross-current gradient ($\partial\overline{q}/\partial s$), between the depth of $\partial\overline{q}/\partial s$ sign change (from positive to negative) and the mean depth of BC–IWBC system flow reversal. The eddy signal was then observed to propagate upward, draining potential energy from the BC, until it reached the surface 30 days after its formation.

Considering the fact that the mean depth of BC–IWBC flow reversal in the model was deeper, compared to that observed by da Silveira et al. (2008), it is possible that, in the real ocean, the depth of negative $\partial\overline{q}/\partial s$ in this region is located at shallower depths. According to these

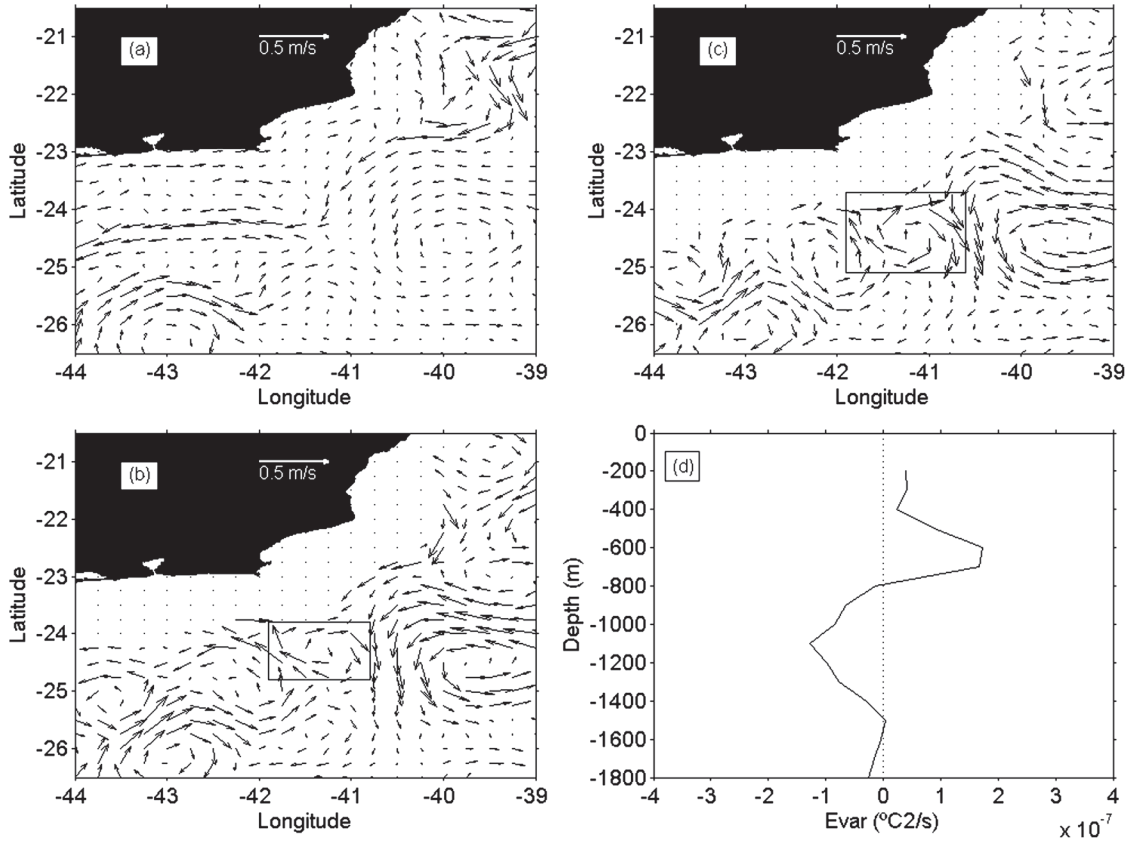

FIG. 12. As in Fig. 9, but for day 30. The rectangle highlights the eddy at 400 and 700 m.

authors, the depth of $\partial\overline{q}/\partial s$ sign change, from positive to negative, is 350 m, which would mean a shallower depth of eddy origin and a shorter time for eddy signal propagation from the origin depth to the surface than seen here.

Pedlosky (1979) demonstrated that the energy flux occurs at the depth where the perturbation phase speed and the mean flow magnitudes are similar (steering level). According to Johns (1988), to satisfy the conditions for internal baroclinic instability, the steering level should be in the negative region of $\partial\overline{q}/\partial s$ but close to the depth of sign change. The peak of energy flux to the perturbation (E_{var} positive peak) occurred at 600 m, while the $\partial\overline{q}/\partial s$ sign change, from positive to negative, is around 450 m. The relation between energy flux and the vertical profile of $\partial\overline{q}/\partial s$ found in this work is, therefore, in agreement with the theory.

The results suggest the following sequence of events during the formation cycle of the Cabo Frio cyclonic eddy: 1) a well-defined southwestward-flowing BC in the beginning of the period, with a baroclinically unstable profile of $\partial\overline{q}/\partial s$; 2) energy flux from the BC to the perturbation at the depth of negative $\partial\overline{q}/\partial s$, close to the depth of $\partial\overline{q}/\partial s$ sign inversion; 3) current destabilization and meandering at this depth; 4) formation and growth of the cyclonic eddy; 5) potential energy flux progressively shallower; 6) propagation of the eddy signal upward throughout the period, tilted against the mean vertical shear; and 7) stabilization of the water column.

The tilting of the perturbation in the opposite direction of the BC vertical shear and the eddy formation related to the APE flux from the mean flow toward the perturbation at depths below the surface layer strongly support the hypothesis that the origin of cyclonic eddies off CF is associated with internal baroclinic instability.

We speculate that the water column stabilization found at the end of the cycle could have been caused by the IWBC in a role similar to the deep western boundary current in the North Atlantic, described by Spall (1996). Throughout the study period, the depth of flow inversion oscillated significantly, indicating the rise of IWBC. On reaching shallower depths, it would invert the energy flux, intensifying the mean flow. More studies on space and time variability of the IWBC should be done to confirm that.

In spite of being well based, the physical study of a single eddy is not enough to extend its characteristics to all eddies in the CF region. Preliminary analysis of the entire simulation period, however, shows that at least

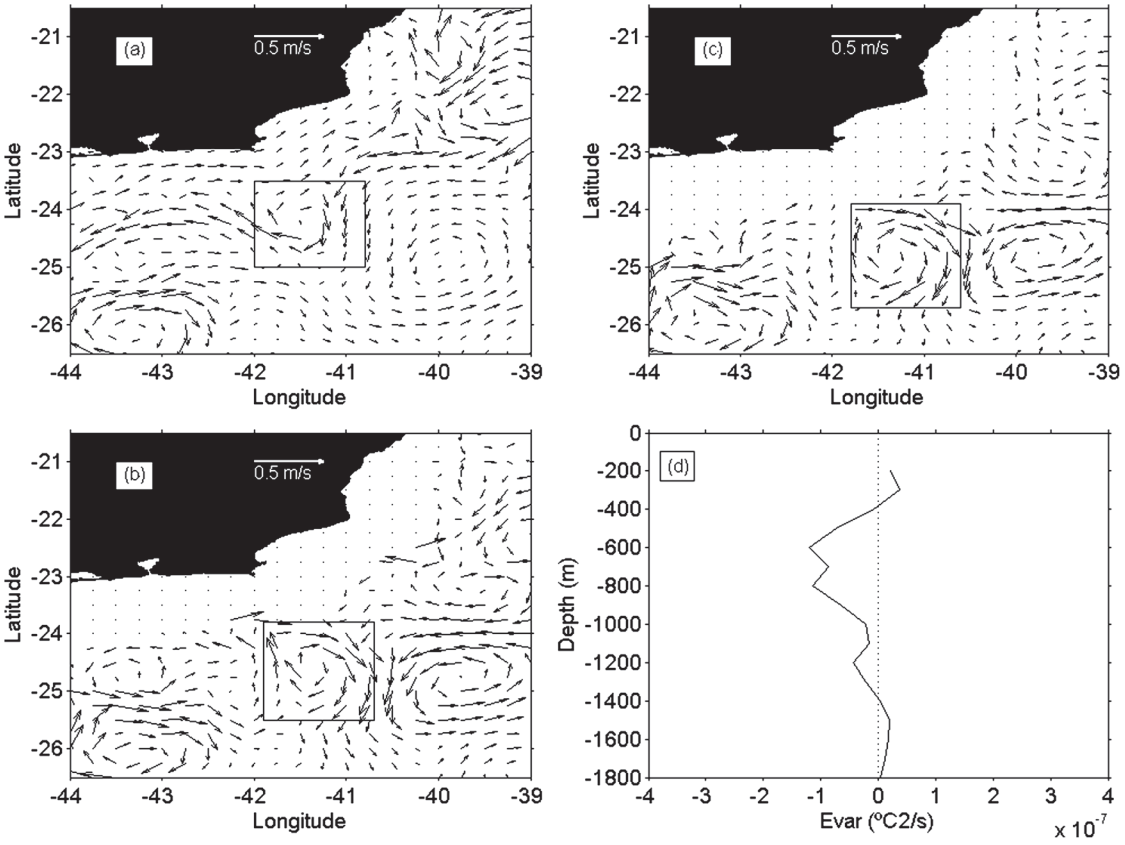

FIG. 13. As in Fig. 9, but for day 40. The rectangle highlights the eddy at the three depths.

one other isolated cyclonic eddy was formed in intermediate depths, indicating that the mechanism observed in this study should be relevant to the formation of the CF cyclonic eddy. Eddies that appear in cyclonic and anticyclonic pairs, respectively, in the west and east sides of the BC, which are also common in the region, seem to have a distinct origin, as their appearance in the model solution occurred simultaneously throughout the first kilometer of the water column, indicating barotropic behavior. Da Silveira et al. (2000) suggest that these pairs of eddies are generated by barotropically unstable topographic Rossby waves. The CF region would present, therefore, eddies that are generated with baroclinic instability predominance or barotropic instability predominance. The former type would follow the dynamics observed herein.

Acknowledgments. This work is partially supported by the Petroleum National Agency (ANP, Brazil), through the Human Resource Formation Program (PRH-02). Prof. Coutinho acknowledges partial support of CNPq. Computing resources were provided by the Laboratory of Computing Methods in Engineering (LAMCE), Department of Civil Engineering, and the Center for Parallel Computing (NACAD), both at Alberto Luiz Coimbra Institute Graduate School and Research in Engineering (COPPE), Federal University of Rio de Janeiro, Brazil.

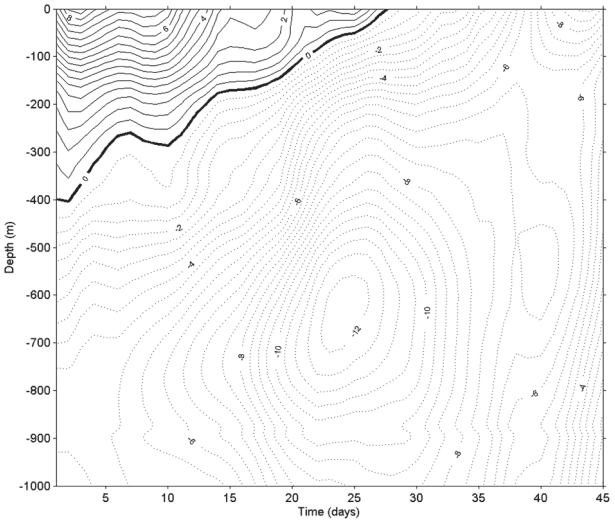

FIG. 14. Time variation of the vertical profile of relative vorticity ($s^{-1} \times 10^{-6}$) for the area of origin of the eddy (24°–24.5°S, 41°–41.5°W). Negative vorticity indicates a cyclonic gyre.

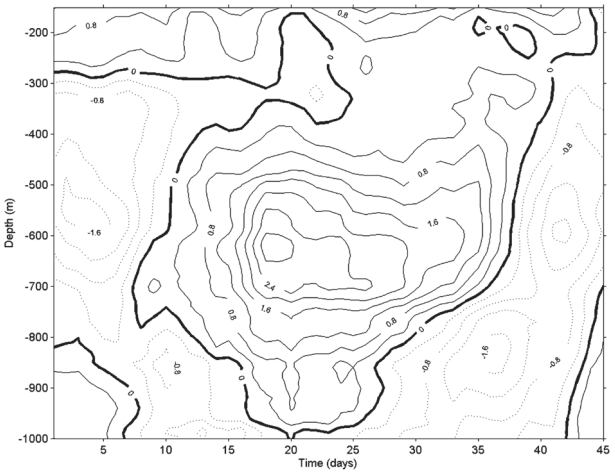

FIG. 15. Time variation of the vertical profile of E_{var} (normalized for the dotted polygon area in Fig. 1), in $^{\circ}\text{C}^2\ \text{s}^{-1} \times 10^{-7}$. Positive E_{var} indicates an energy flux toward perturbation.

REFERENCES

Barnier, B., P. Marchesiello, A. P. De Miranda, J. M. Molines, and M. Coulibaly, 1998: A sigma-coordinate primitive equation model for studying the circulation in the South Atlantic. Part I: Model configuration with error estimates. *Deep-Sea Res. I,* **45,** 543–572.

Blumberg, A. F., and G. L. Mellor, 1987: A description of a three dimensional coastal ocean circulation model. *Three-Dimensional Coastal Ocean Models,* N. Heaps, Ed., Amer. Geophys. Union, 208 pp.

Campos, E. J. D., J. E. Gonçalves, and Y. Ikeda, 1995: Water mass characteristics and geostrophic circulation in the South Brazil Bight: Summer of 1991. *J. Geophys. Res.,* **100** (C9), 18 537–18 550.

——, Y. Ikeda, B. M. Castro, S. A. Gaeta, J. A. Lorenzzetti, and M. R. Stevenson, 1996: Experiment studies circulation in the western South Atlantic. *Eos, Trans. Amer. Geophys. Union,* **77,** 253.

da Silveira, I. C. A., A. K. Schmidt, E. J. D. Campos, S. S. Godoi, and Y. Ikeda, 2000: The Brazil Current off Brazilian east coast. *Braz. J. Oceanogr.,* **48** (2), 171–183.

——, L. Calado, B. M. Castro, M. Cirano, J. A. M. Lima, and A. S. Mascarenhas, 2004: On the baroclinic structure of the Brazil Current–Intermediate Western Boundary Current system at 22°–23°S. *Geophys. Res. Lett.,* **31,** L14308, doi:10.1029/2004GL020036.

——, J. A. M. Lima, A. C. K. Schmidt, W. Ceccopieri, A. Sartori, C. P. F. Francisco, and R. F. C. Fontes, 2008: Is the meander growth in the Brazil current system off Southeast Brazil due to baroclinic instability? *Dyn. Atmos. Oceans,* **45,** 187–207.

Ezer, T., H. Arango, and A. F. Shchepetkin, 2002: Developments in terrain-following ocean models: Intercomparisons of numerical aspects. *Ocean Modell.,* **4,** 249–267.

Flather, R. A., 1976: A tidal model of the north-west European continental shelf. *Mem. Soc. Roy. Sci. Liège,* **6** (10), 141–164.

Garfield, N., 1990: The Brazil Current at subtropical latitudes. Ph.D. thesis, University of Rhode Island, 121 pp.

Gwilliam, C. S., 1995: The OCCAM Global Ocean Model. *Coming of Age (The Proceedings of the Sixth ECMWF Workshop on the Use of Parallel Processors in Meteorology),* G.-R. Hoffmann and N. Kreitz, Eds., World Scientific, 446–454.

Johns, W. E., 1988: One-dimensional baroclinically unstable waves on the Gulf Stream potential vorticity gradient near Cape Hatteras. *Dyn. Atmos. Oceans,* **11,** 323–350.

Lorenzzetti, J. A., M. R. Stevenson, C. L. Silva Jr., and R. B. Souza, 1994: Behavior of a semi-permanent eddy as observed from AVHRR images and WOCE drifters. *Extended Abstracts, The South Atlantic – Present And Past Circulation Symp.,* Bremen, Germany, Universitat Bremen, 83–84.

Mascarenhas, A. S., Jr., L. B. Miranda, and N. J. Rock, 1971: A study of the oceanographic conditions in the region of Cabo Frio. *Fertility in the Sea,* J. D. Costlow, Jr., Ed., Vol. 1, Gordon & Breach, 285–308.

NOAA, 1988: Digital relief of the surface of the Earth. NOAA/National Geophysical Data Center Data Announcement 88-MGG-02, Boulder, CO.

Pedlosky, J., 1979: *Geophysical Fluid Dynamics*. Springer, 624 pp.

Peterson, R. G., and L. Stramma, 1991: Upper-level circulation in the South Atlantic Ocean. *Prog. Oceanogr.,* **26,** 1–73.

Reid, J. L., 1989: On the total geostrophic circulation of the South Atlantic Ocean: Flow patterns, tracers and transports. *Prog. Oceanogr.,* **23,** 149–244.

Schmid, C., H. Schafer, G. Podesta, and W. Zenk, 1995: The Vitória eddy and its relation to the Brazil Current. *J. Phys. Oceanogr.,* **25,** 2532–2546.

Signorini, S. R., 1978: On the circulation and the volume transport of the Brazil Current between São Tomé and Guanabara Bay. *Deep-Sea Res.,* **25,** 481–490.

Sommerfeld, A., 1949: *Partial Differential Equations in Physics*. Academic Press, 335 pp.

Spall, M. A., 1996: Dynamics of the Gulf Stream/deep western boundary current crossover. Part II: Low-frequency internal oscillations. *J. Phys. Oceanogr.,* **26,** 2169–2182.

Stevenson, M. R., 1996: Recirculation of the Brazil Current south of 23°S. *International WOCE Newsletter,* No. 22, WOCE International Project Office, Southampton, United Kingdom, 30–32.

Zavatarelli, M., and G. L. Mellor, 1995: A numerical study of the Mediterranean Sea circulation. *J. Phys. Oceanogr.,* **25,** 1384–1414.